Nanoscale

COMMUNICATION

View Article Online
View Journal | View Issue

Cite this: *Nanoscale*, 2015, **7**, 13358

Received 6th May 2015,
Accepted 11th June 2015

DOI: 10.1039/c5nr02959g

www.rsc.org/nanoscale

Reversible control of pore size and surface chemistry of mesoporous silica through dynamic covalent chemistry: philicity mediated catalysis†

Dheeraj Kumar Singh, B. V. V. S. Pavan Kumar and M. Eswaramoorthy*

Here, we report the synthesis of adaptive hybrid mesoporous silica having the ability to reconfigure its pore properties such as pore size and philicity in response to the external environment. Decyl chains were reversibly appended to the pore walls of silica through imine motifs as dynamic covalent modules to switch the pore size and philicity in response to pH. This switching of pore properties was used to gate the access of reactants to the gold nanoparticles immobilized inside the nanopores, thus enabling us to turn-on/turn-off the catalytic reaction. The use of such dynamic covalent modules to govern pore properties would enable the realization of intelligent hybrids capable of controlling many such chemical processes in response to stimuli.

Controlling the surface chemistry of nanopores through chemical modifications is paramount to effectively utilize mesoporous silicas in catalysis,[1,2] electrochemistry,[3] ion-gating,[4] drug delivery,[5] separation,[6,7] chiral recognition[8] *etc*. Though both covalent and supramolecular strategies[9,10] are adopted for functionalization, covalent tethering of functional moieties dominates the surface chemistry of these materials as they offer rigidity to the organic linkers. However, covalent systems are predominantly irreversible in nature, lack dynamism and are largely limited to a single-purpose once functionalized. On the other hand, the supramolecular approach, though reversible and dynamic, lacks the rigidity of covalent functionalities as their interactions are often weak due to their non-covalent nature. Functionalization which combines both the rigidity of covalent linkers and the reversibility of supramolecular systems is expected to give new dimensions to the applicability of these porous materials. In this context, the emergence of dynamic covalent chemistry[11,12] has added a new paradigm to synthetic chemistry with the concept of assembly and disassembly,[13] much like living systems, in response to the external environment.[14] Modifications of pores by such dynamic covalent motifs where the cleavage and bond formation occur reversibly (on exposure to the external stimuli) would enable post-synthetic reconfiguration of several pore properties like pore-size, philicity and surface charge. Such reversible stimuli responsive control over pore properties can help realize systems with switchable catalytic, adsorption, ion-transport and drug release properties.

To demonstrate the importance of dynamic covalent motifs in modifying the pore properties reversibly, we have selected primary amine functionalized mesoporous silica, SBA-15 (SBA),[15] which is capable of forming dynamic imine bonds with aldehydes.[11,12] At high pH the condensation between amines and aldehydes leads to an imine bond which undergoes reversible cleavage at low pH. We have chosen *p*-hydroxybenzaldehyde appended with a decyl chain, 4-decyloxybenzaldehyde (4-DB), as a pore modifier to simultaneously modify the pore size and philicity in imine formation. The dynamic nature of imine bonds was exploited to reversibly switch the pore size and philicity of SBA (Scheme 1) which in turn was used to control the kinetics of catalytic reactions within the confined pores. Such modulation of kinetics, induced by philicity changes in pores, allows greater control over catalytic reactions, enabling switching behavior between on and off states.[16,17]

Monodisperse rods of mesoporous silica SBA[18] (Fig. 1a and S1†) were synthesized according to a reported procedure and functionalized with aminopropyl groups using a silane strategy *via* (3-aminopropyl)triethoxysilane (APTES) to form SBA-AM (Fig. S2†). Powder X-ray diffraction (PXRD) patterns of SBA and SBA-AM (Fig. S3†) show well resolved low angle peaks indicating retention of the mesostructure after silanization.[19] N_2 adsorption–desorption isotherms recorded on SBA and SBA-AM at 77 K exhibited type IV behavior (Fig. 1c), typical of mesoporous materials.[20] The pore size distribution calculated

Nanomaterials and Catalysis Lab, Chemistry and Physics of Materials Unit, Jawaharlal Nehru Centre for Advanced Scientific Research (JNCASR), Jakkur P.O., Bengaluru 560064, India. E-mail: eswar@jncasr.ac.in; Fax: +(91) 80-2208-2766

†Electronic supplementary information (ESI) available. See DOI: 10.1039/c5nr02959g

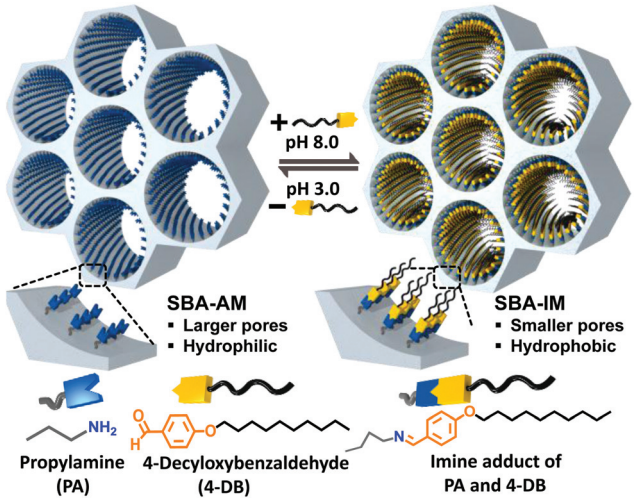

Scheme 1 Illustration depicting reversible engineering of the pore size and philicity of mesoporous SBA *via* dynamic covalent chemistry triggered by changes in pH.

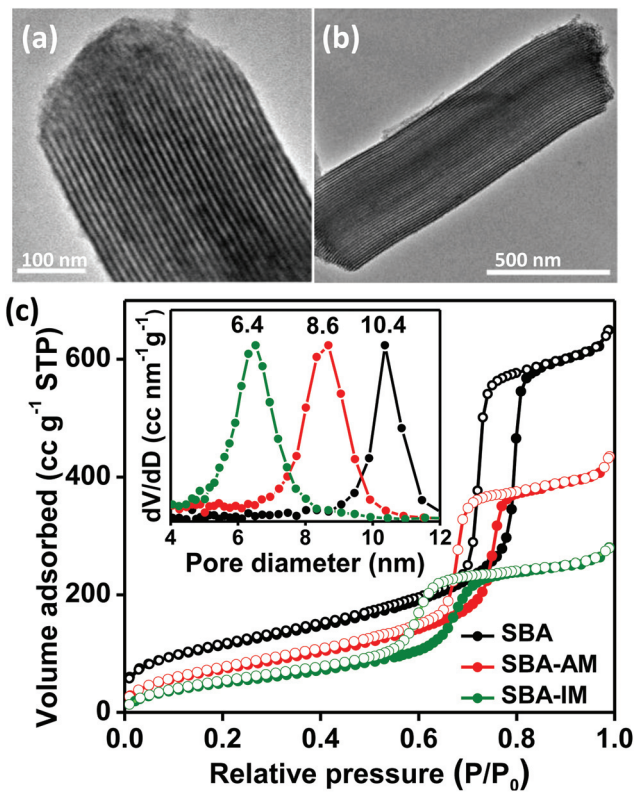

Fig. 1 (a) and (b) are TEM images of SBA and SBA-IM respectively showing well aligned pores before and after functionalization. (c) N_2 adsorption–desorption isotherms (inset shows the corresponding pore size distribution calculated by using the BJH method) of pristine and functionalized SBA.

using the Barrett–Joyner–Halenda (BJH)[21] method showed a decrease in the pore size from 10.4 nm to 8.6 nm on functionalization of SBA with aminopropyl groups (inset of Fig. 1c). Fourier transform infrared (FTIR) spectra of SBA-AM showed sp^3 C–H stretching vibrations in the region 2900–3000 cm^{-1}, indicating the presence of alkyl chains (Fig. S4†). The density of amine groups on the surface of pore walls, as calculated from thermogravimetric (Fig. S5†) and elemental analysis (Table S1†), was found to be around 1.6 mmol g^{-1} for SBA-AM. The pore modifier, 4-DB (4-decyloxybenzaldehyde), was then linked to amine groups in SBA-AM through the imine bond to give SBA-IM (Fig. S2†). The PXRD patterns (Fig. S3†) of SBA-IM show retention of mesostructural ordering on imine functionalization which was further confirmed by FESEM (Fig. S6†) and TEM (Fig. 1b) images. N_2 adsorption–desorption isotherms of SBA-IM show retention of the type IV isotherm (Fig. 1c) with a sharp decrease in the pore size of about 2.2 nm (from 8.6 nm of SBA-AM to about 6.4 nm for SBA-IM (inset of Fig. 1)), which is commensurate with twice the length of 4-DB. The strong hydrophobicity of pores associated with the attachment of the long decyl chain is revealed by the poor uptake of water in the water sorption isotherm which is in sharp contrast to the high water uptake observed for SBA-AM at a P/P_0 around 0.77 (Fig. 2). The absorption band associated with the C=N (imine stretching) bond at 1642 cm^{-1} (ref. 22 and 23) as well as for the aromatic stretching modes at 1605 cm^{-1} and 1511 cm^{-1} in the FTIR spectra of SBA-IM further confirms the binding of 4-DB to the pore walls through imine functionalization (Fig. S4†). Additionally, the long alkyl chain associated with 4-DB in SBA-IM shows intense peaks for sp^3 C–H stretching in the region 2900–3000 cm^{-1} as compared to SBA-AM (Fig. S4†). The degree of imine functionalization calculated from TGA (Fig. S5†) and elemental analysis was found to be around 0.9 mmol g^{-1} (Table S1†).

The dynamic nature of the imine bond (formation and cleavage at high and low pH respectively) and its influence in reversibly controlling the pore size and philicity of mesoporous

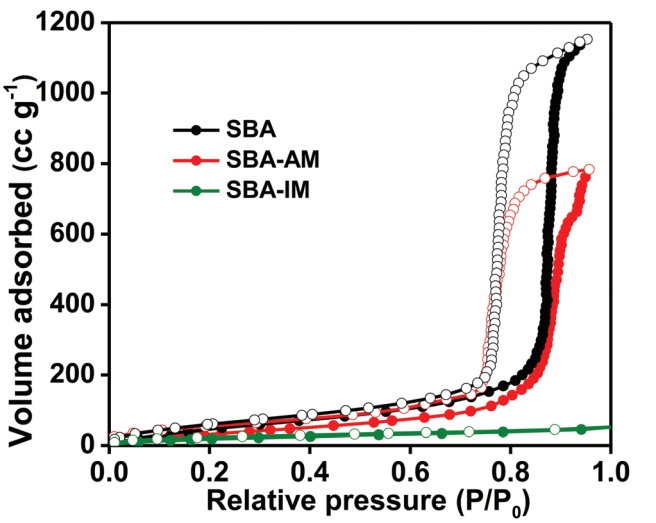

Fig. 2 Water adsorption–desorption isotherms of SBA, SBA-AM and SBA-IM, indicating negligible uptake of water by SBA-IM.

silica was demonstrated by dispersing SBA-IM in a water–ethanol mixture (6 : 5 v/v) at two different pH values (pH 8 and 3, Fig. S7†). At pH 8, the imine bonds are stable and do not undergo any cleavage and thus the pore size remains the same, 6.4 nm (Fig. 3, SBA-IM-R1). FTIR spectra of SBA-IM kept at pH 8 for 16 h (SBA-IM-R1) shows a similar pattern to that of as-prepared SBA-IM confirming the retention of imine bonds at pH 8 (Fig. S8†). However, on changing the pH from 8 to 3, imine bonds undergo cleavage ensuring the regeneration of SBA-AM, designated as SBA-AM-R1. FTIR spectra of SBA-AM-R1 (Fig. S9†) did not show a signature C=N stretch or aromatic (of benzaldehyde) ring breathing vibrations, indicating that the cleavage of imine bonds resulted in the detachment of 4-DB from the pore walls. The pore size distribution calculated from the N_2 adsorption–desorption isotherms was around 8.6 nm which is similar to that of SBA-AM supporting the cleavage of imine bonds in acidic medium (Fig. 3). A water–ethanol mixture was necessary to ensure the wetting of hydrophobic pores of SBA-IM to facilitate the cleavage of imine bonds at pH 3 to form SBA-AM-R1. On changing the pH of the medium back to 8 (in which 4-DB, resulting from the cleavage of the imine bond at pH 3, was present), the 4-DB present in the solution reacted with the amine groups of the SBA-AM-R1 to form imine bonds again, SBA-IM-R2, in 16 h time. Pore size distribution calculated from N_2 adsorption–desorption isotherms (Fig. 3) showed a decrease in size back to 6.5 nm from 8.6 nm, similar to that of SBA-IM, suggesting the reformation of imine bonds in basic medium. This was further evident from the re-emergence of peaks in the FTIR spectra corresponding to C=N stretching (1642 cm^{-1}), as well as aromatic ring and alkyl sp^3 C–H stretching vibrations (Fig. S10†). Then keeping the SBA-IM-R2 in the same medium at pH3 for 16 h hydrolyses the imine bonds and as a result the pore size changes back to 8.6 nm similar to that of SBA-AM (denoted as SBA-AM-R2 in Fig. 3). Furthermore, SBA-AM-R2 has functionalities similar to that of SBA-AM as confirmed by FTIR spectra (Fig. S11†). The FESEM and TEM micrographs show the retention of mesostructural pore ordering after two pH cycles (Fig. S12 a–d†).

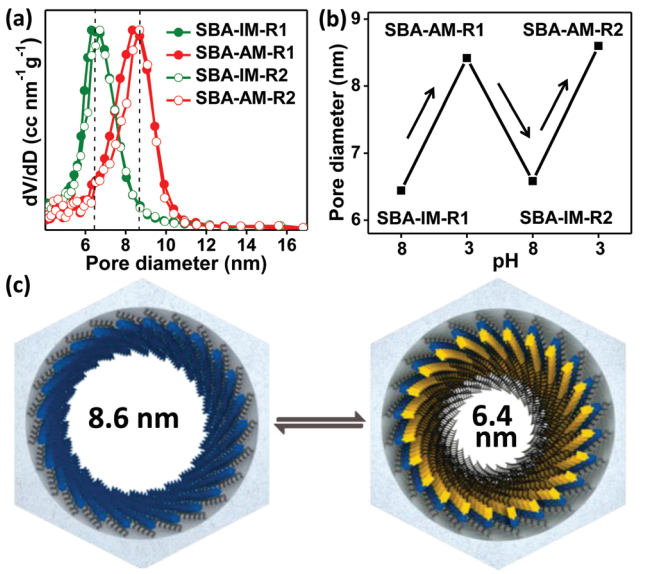

Fig. 3 (a) Normalized pore size distributions showing switching of pore size with pH. (b) Variation of pore size on cycling the pH between 3 and 8, showing good reversibility. (c) Schematic showing the decrease in pore size on forming imine bonds (with 4-DB) at pH 8.

To illustrate the effect of pore philicity (hydrophobic/hydrophilic) in regulating the access of the reactants to the catalytic sites and hence the catalytic activity, reduction of *p*-nitrophenol over gold nanoparticles embedded inside the SBA pores was used as a model reaction. Mesoporous silica, SBA containing gold nanoparticles, selectively grown inside the pores,[24] SBA-Au was used as the starting material. Selective growth of Au nanoparticles inside the pores of SBA was achieved through the double-solvent (*n*-hexane–water) approach[25] reported in the literature. Subsequent functionalization with APTES and 4-DB successively resulted in SBA-Au-AM and SBA-Au-IM, respectively. PXRD patterns (Fig. S13†), N_2 adsorption–desorption isotherms (Fig. S14†) and FTIR spectra (Fig. S15†) of SBA-Au, SBA-Au-AM and SBA-Au-IM were similar to those of SBA, SBA-AM and SBA-IM, respectively. TEM micrographs (Fig. S16a–b†) show gold nanoparticles immobilized inside the pores and the statistical analysis of a large number of particles (170 particles) reveals the mean diameter of Au nanoparticles to be around 6.3 nm (Fig. S16c†) which is less than the pore diameter. The gold loading was quantified using ICP-MS which was found to be around 0.2 wt%.

Catalytic studies showed that reduction of *p*-nitrophenol in aqueous medium occurred only on SBA-Au-AM but not on SBA-Au-IM (Fig. 4a–d). The hydrophilic pores of SBA-Au-AM are easily wetted by water which enable the access of the reactants to the gold nanoparticles located inside the pores (Fig. 4a). On the other hand, the hydrophobic environment created by the decyl chains of SBA-Au-IM resulted in dewetting of pores in aqueous media and this inhibited the reactants from reaching the catalytically active gold nanoparticles (Fig. 4c). In order to aid the access to the pores in SBA-Au-IM, the catalytic studies were performed in a water–ethanol mixture (Fig. S17a–d†). Nevertheless, the gold nanoparticles in SBA-Au-IM were still unable to show catalytic activity. We believe this could possibly be due to the selective entry of ethanol (along with reactant) into the hydrophobic pores leaving behind water solubilized $NaBH_4$ outside (Fig. S17c–d†).

Moreover, the solubility of $NaBH_4$ in ethanol is poor and shows no catalytic reduction in pure ethanol medium. Separate experiments carried out with Au nanoparticles loaded SBA showed no reduction of *p*-nitrophenol with $NaBH_4$ when the medium was pure ethanol (Fig. S18†). The reduction occurred only when the medium was water or water–ethanol mixture though the kinetics of reduction was slower in water–ethanol medium as compared to water (Fig. S18†). A similar trend was found even for bare gold nanoparticle mediated reduction of *p*-nitrophenol (Fig. S19†). On the other hand, SBA-Au-AM did not show any catalytic activity in water–ethanol medium

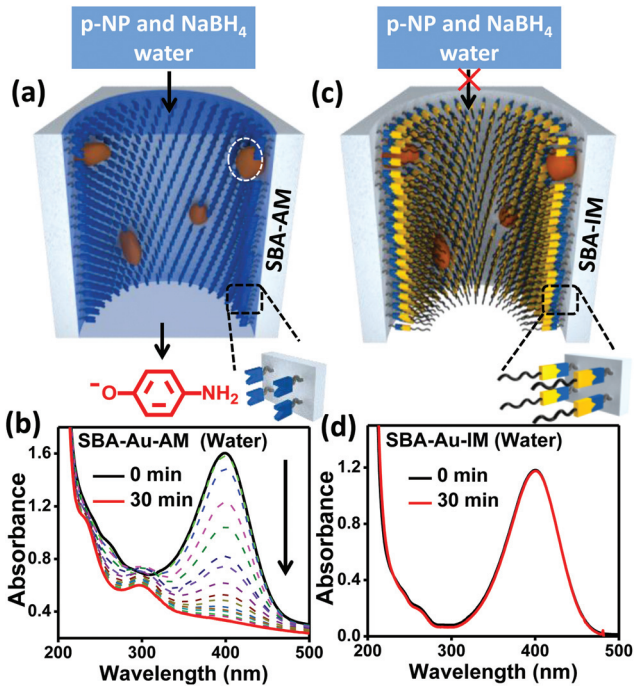

Fig. 4 Catalysis in water medium. (a) Schematic showing gold nanoparticles (encircled in white) immobilized in the pores of SBA-Au-AM, carrying out catalytic reduction of *p*-nitrophenol. (b) UV-Vis spectra indicating complete reduction of *p*-nitrophenol to *p*-aminophenol within 30 min by SBA-Au-AM (arrow indicating the decrease in intensity with time). (c) Illustration showing the absence of catalytic activity due to dewetting of the pores caused by hydrophobicity of SBA-Au-IM. (d) Corresponding UV-Vis spectra indicating no catalytic reduction.

(Fig. S17a–b†) similar to that of SBA-Au-IM (Fig. S17c–d†). This is in sharp contrast to the catalytic activity observed for SBA-Au-AM in aqueous medium. This could be rationalized by considering the fact that high pH (around 11) associated with the use of $NaBH_4$, deprotonates the propylammonium ions ($pK_a \sim 8$) making them neutral. This would create a pseudo hydrophobic environment inside the pores leading to preferential pore entry of ethanol and inhibition of catalytic activity.

In conclusion, we have developed a dynamic organic–inorganic hybrid material which combines the rigidity and stability of an inorganic framework with the reversibility of dynamic covalent (imine based) systems. These materials were shown to exhibit reversible switching of pore size and philicity which was used to control the access of the reactants to the interior of the pores. The dynamic control exerted by these imine-based covalent systems on the nature of pores (with respect to external stimuli) was exploited to regulate the catalytic reduction of *p*-nitrophenol within the nanopores. We believe that the methodology employed here can be extended to generate a host of new covalent functional materials capable of showing functional reorganization in response to external stimuli truly mimicking the role of adaptive materials.

Acknowledgements

We thank Prof. C.N.R. Rao for his encouragement and support, N. Sikdar and A. Chakraborty for water sorption measurements. D.K.S. and B.V.V.S.P.K. thank CSIR for fellowships and B.V.V.S.P.K. is also grateful for a Sheikh Saqr Junior Fellowship. D.K.S. and B.V.V.S.P.K. thank M. Kumar for discussions.

References

1 H. T. Chen, S. Huh, J. W. Wiench, M. Pruski and V. S. Y. Lin, *J. Am. Chem. Soc.*, 2005, **127**, 13305–13311.
2 L. Shang, T. Bian, B. Zhang, D. Zhang, L.-Z. Wu, C. H. Tung, Y. Yin and T. Zhang, *Angew. Chem., Int. Ed.*, 2014, **53**, 250–254.
3 A. Walcarius, *Chem. Soc. Rev.*, 2013, **42**, 4098–4140.
4 R. Fan, S. Huh, R. Yan, J. Arnold and P. Yang, *Nat. Mater.*, 2008, **7**, 303–307.
5 N. Singh, A. Karambelkar, L. Gu, K. Lin, J. S. Miller, C. S. Chen, M. J. Sailor and S. N. Bhatia, *J. Am. Chem. Soc.*, 2011, **133**, 19582–19585.
6 X. Feng, G. E. Fryxell, L. Q. Wang, A. Y. Kim, J. Liu and K. M. Kemner, *Science*, 1997, **276**, 923–926.
7 X. Pan, Y. Chen, P. Zhao, D. Li and Z. Liu, *Angew. Chem., Int. Ed.*, 2015, **54**, 6173–6176.
8 P. Paik, A. Gedanken and Y. Mastai, *Microporous Mesoporous Mater.*, 2010, **129**, 82–89.
9 I. Slowing, B. G. Trewyn and V. S. Y. Lin, *J. Am. Chem. Soc.*, 2006, **128**, 14792–14793.
10 M. Sardan, A. Yildirim, D. Mumcuoglu, A. B. Tekinay and M. O. Guler, *J. Mater. Chem. B*, 2014, **2**, 2168–2174.
11 S. J. Rowan, S. J. Cantrill, G. R. L. Cousins, J. K. M. Sanders and J. F. Stoddart, *Angew. Chem., Int. Ed.*, 2002, **41**, 898–952.
12 S. Fujii and J. M. Lehn, *Angew. Chem., Int. Ed.*, 2009, **48**, 7635–7638.
13 C. B. Minkenberg, L. Florusse, R. Eelkema, G. J. M. Koper and J. H. van Esch, *J. Am. Chem. Soc.*, 2009, **131**, 11274–11275.
14 N. Hafezi and J. M. Lehn, *J. Am. Chem. Soc.*, 2012, **134**, 12861–12868.
15 D. Zhao, J. Feng, Q. Huo, N. Melosh, G. H. Fredrickson, B. F. Chmelka and G. D. Stucky, *Science*, 1998, **279**, 548–552.
16 G. Wang, K. Kuroda, T. Enoki, A. Grosberg, S. Masamune, T. Oya, Y. Takeoka and T. Tanaka, *Proc. Natl. Acad. Sci. U. S. A.*, 2000, **97**, 9861–9864.
17 Y. Wei, S. Han, J. Kim, S. Soh and B. A. Grzybowski, *J. Am. Chem. Soc.*, 2010, **132**, 11018–11020.
18 A. Sayari, B.-H. Han and Y. Yang, *J. Am. Chem. Soc.*, 2004, **126**, 14348–14349.
19 J. C. Doadrio, E. M. B. Sousa, I. Izquierdo-Barba, A. L. Doadrio, J. Perez-Pariente and M. Vallet-Regi, *J. Mater. Chem.*, 2006, **16**, 462–466.

20 K. S. W. Sing, D. H. Everett, R. A. W. Haul, L. Moscou, R. A. Pierotti, J. Rouquerol and T. Siemieniewska, *Pure Appl. Chem.*, 1985, **57**, 603–619.
21 E. P. Barrett, L. G. Joyner and P. P. Halenda, *J. Am. Chem. Soc.*, 1951, **73**, 373–380.
22 C. Wang, G. Wang, Z. Wang and X. Zhang, *Chem. – Eur. J.*, 2011, **17**, 3322–3325.
23 K. Acharyya, S. Mukherjee and P. S. Mukherjee, *J. Am. Chem. Soc.*, 2012, **135**, 554–557.
24 Q. L. Zhu, J. Li and Q. Xu, *J. Am. Chem. Soc.*, 2013, **135**, 10210–10213.
25 A. Aijaz, A. Karkamkar, Y. J. Choi, N. Tsumori, E. Rönnebro, T. Autrey, H. Shioyama and Q. Xu, *J. Am. Chem. Soc.*, 2012, **134**, 13926–13929.

